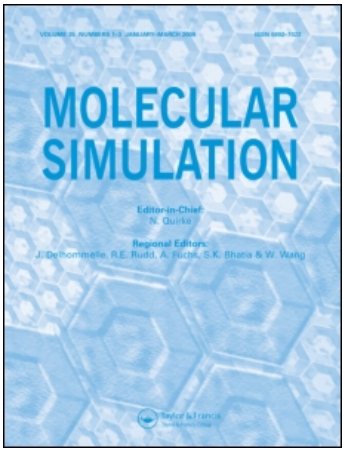

Molecular Simulation
Publication details, including instructions for authors and subscription information:
http://www.informaworld.com/smpp/title~content=t713644482

Exploring the effects of different immersion environments on the growth of gold nanostructures

G. Grochola[a]; I. Snook[a]; D. Chui[a]; S. P. Russo[a]
[a] Applied Physics, School of Applied Sciences, RMIT University, Melbourne, Australia

To cite this Article Grochola, G. , Snook, I. , Chui, D. and Russo, S. P.(2006) 'Exploring the effects of different immersion environments on the growth of gold nanostructures', Molecular Simulation, 32: 15, 1255 — 1260
To link to this Article: DOI: 10.1080/08927020600891445
URL: http://dx.doi.org/10.1080/08927020600891445

Molecular Simulation, Vol. 32, No. 15, 30 December 2006, 1255–1260

Taylor & Francis
Taylor & Francis Group

Exploring the effects of different immersion environments on the growth of gold nanostructures

G. GROCHOLA, I. SNOOK*, D. CHUI and S. P. RUSSO

Applied Physics, School of Applied Sciences, RMIT University, Melbourne, Australia

(Received July 2006; in final form July 2006)

Even though Au crystallizes only as a simple FCC structure in bulk there have been many different and fascinating structures discovered experimentally for Au on the nanoscale. Unfortunately, for Au a direct *ab-initio* approach in studying dynamic growth mechanisms of nanostructures is prohibitively expensive from a computational perspective, so here we use methods based on accurate semi-empirical, many-body potentials whose parameters are obtained from a combination of empirical and *ab-initio* data as a viable alternative. We show that this method when combined with molecular dynamics may be used to simulate the growth of Au particles in a bath of solvent atoms (either in a gaseous or liquid state) which results in structures of a range of different morphologies. An analysis of the results indicates what characteristics of the solvent and its interactions are important in determining these different morphologies.

Keywords: Gold nanostructures; Molecular dynamics; Growth mechanisms; Nanoparticles

1. Introduction

Because of the combination of different factors, e.g. the ability of C to form several distinctly different bonding arrangements, the ability of different bonding arrangements to co-exist [1] and the instability some surfaces, there are many possible nano-carbon structures which may be produced [2–6]. It is possible to study many of these systems by *ab-intio* and semi-empirical quantum mechanical methods. By contrast Au forms a very simple FCC lattice in the bulk solid phase, so at first sight it might appear that unlike C, Au might not form very many different structures at the nano-level. The only unusual aspect of solid, bulk Au is that its surfaces reconstruct rather interestingly [7,8]. However, in contrast to the behavior in bulk a number of fascinating different structures have been observed for Au at the nanoscale. Particles of different morphologies may be grown by using different growth conditions, e.g. by growth in the vapour phase in the presence of an inert gas or in solution with the presence of surfactants [9–11]. Properties of nanoparticles are known to depend on their shape and size, and specific applications require tight control of batch distributions. Hence it is of paramount importance to understand the controlling factors which determine the growth of the different morphologies which have been observed. This should enable better understanding of how to grow particles of a desired morphology and, thus, of particles having desired properties.

However, as Au has many more active electrons than C (and also relativistic effects may be important) *ab-initio* quantum mechanical methods are much more computationally expensive to apply to Au structures than to C structures. Thus, we have used accurate empirical potentials in conjunction with a molecular dynamics (MD) model to simulate the growth of Au nanoparticles in a variety of different environments.

The parameters of Au–Au interaction potential was previously obtained from a combination of empirical and *ab-initio* data [12] using the force matching method. The form of the potential used for Au–Au interactions was an embedded atom model (EAM) type which uses the sum of a pair potential and a many-body environment dependent term. The Au-solvent and solvent–solvent potentials were modeled in a variety of ways to represent different classes of adsorbent as discussed in subsequent sections of this paper. A variety of different growth morphologies were obtained depending on the physical state of the system and on the form of the adsorbent model.

*Corresponding author. Email: ian.snook@rmit.edu.au

Molecular Simulation
ISSN 0892-7022 print/ISSN 1029-0435 online © 2006 Taylor & Francis
http://www.tandf.co.uk/journals
DOI: 10.1080/08927020600891445

2. Method

For growth in liquids we started from a small cell containing a cluster of four central Au atoms immersed in solution. Gold and solution particles were inserted at regular intervals at a fixed ratio into the simulation cell. We used a random search to find suitable holes in solution for insertion of particles. This slightly disrupted the integration of forces, but we found that the velocity Verlet algorithm was robust enough to deal with this. After particle insertion the system once again settled down to a quasi-equilibrium state. We did, however, observe a precaution that atoms should be inserted away from the central cluster. In practice we inserted atoms about every 2000–4000 time steps where the time step Δt was taken to be between 1.0 and 1.5 fs. The gold to adsorbent insertion ratio was fixed in an individual simulation and ranged from 1/1 to 1/5, the velocity Verlet algorithm was used to integrate the equations of motion and a Broughton Thermostat/Barostat used to maintain constant temperature and pressure. Growth in vapour was carried out in a similar fashion except the cell was expanded by a fixed amount each time a gold atom was introduced.

3. Results and discussion

3.1 Simplest adsorbent intermolecular interaction

In the initial simulations we assumed that all adsorbent/Au interactions were purely pair-wise additive Lennard–Jones (LJ) interactions as were all the adsorbent/adsorbent, i.e. the adsorbent atoms did not contribute any electron density to the Au atoms.

Using these interaction potentials we grew Au nanoparticles in the following manner. We firstly choose a LJ liquid immersion medium by specifying the energy parameter $\sigma_{\mathrm{Liq-Liq}}$ and the length parameter $\varepsilon_{\mathrm{Liq-Liq}}$. Next we fixed a specific cross liquid-gold LJ length, $\sigma_{\mathrm{Liq-Gold}}$. With these three values fixed we carried out a set of simulation with increasing cross liquid–gold LJ well depths, $\varepsilon_{\mathrm{Liq-Gold}}$. We then went back and altered $\sigma_{\mathrm{Liq-Gold}}$ carrying out a further set of simulations by varying $\varepsilon_{\mathrm{Liq-Gold}}$. Lastly we varied the liquid immersion medium and re-performed all the sets of simulations. Interaction lengths, σ varied from 2.5 to 3.4 Å, while well depths, ε varied from 0.01 to 0.14 eV.

Firstly, we can note that in general the values of the $\varepsilon_{\mathrm{Liq-Gold}}$ cross well depths needed to be effectively almost solid-like (when taking into consideration $\sigma_{\mathrm{Liq-Gold}}$) before we obtained non-Icosahedral (non-Ih) morphologies. That is, the liquid needed to effectively form a quasi-solid on the surface of nanoclusters for any significant deviations from the appearance of Ih morphologies.

Next we can note that for very strongly adsorbing LJ liquids ($\varepsilon_{\mathrm{Liq-Gold}} = 0.08$ eV) which roughly matched Gold's lattice constant (for the result $\sigma_{\mathrm{Liq-Gold}} = 2.5$ Å, $\sigma_{\mathrm{Liq-Liq}} = 2.5$ Å) we observed some fcc and Marks Decahederal (mDh) nuclei formed (figure 1(a),(b)) with visible ad-atoms and steps, even for small nuclei ($\sim$50 atoms). This was unlike that observed for nuclei grown in vacuum environment which always tended to be polymorphic Ih [13]. It seemed that such a strongly adsorbing liquid stabilized small regions of (100) faces on the fcc nuclei which is unavoidable for roughly spherical internally fcc nanoparticles, unlike the internally multi-twined Ih and "pancake" m-Dh nuclei. Nevertheless these (100) regions remained small as compared to the area of (111) surface. It also seemed the solution easily allowed for shape distortion away from spherical, since non-spherical particles were common. The gold–liquid interfacial surface tension in this case would presumably be very low.

Interestingly, for the above results if we changed only $\sigma_{\mathrm{Liq-Gold}}$ to 3.65 Å then mostly clean† polymorphic Ih nuclei formed (if somewhat elongated/distorted at the

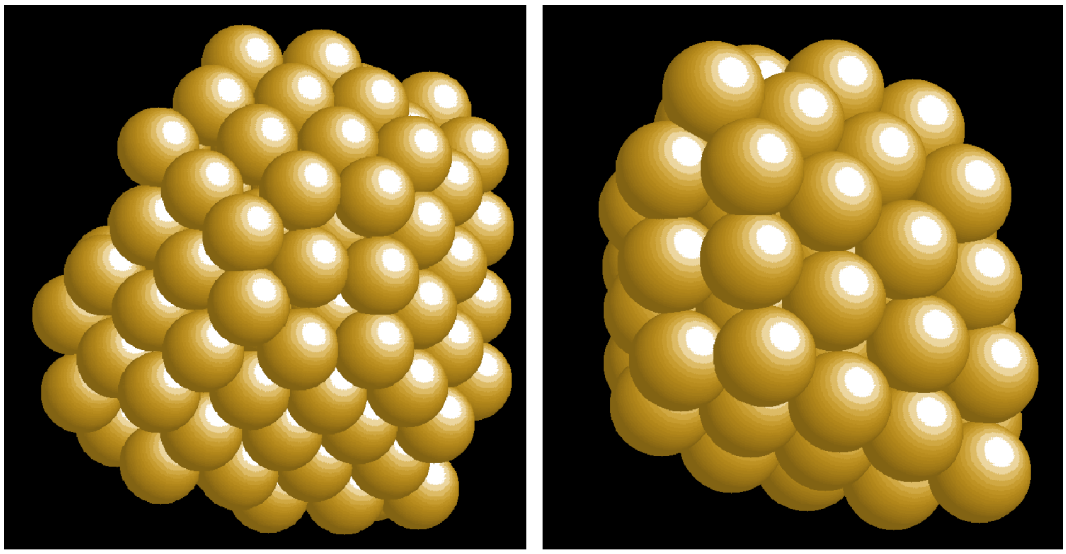

(a) (b)

Figure 1. (a) and (b): FCC nuclei, with the liquid hidden from view, note the very small (100) surface regions.

highest $\varepsilon_{\mathrm{Liq-Gold}}$ due to very low surface tension). Whereas previously for $\sigma_{\mathrm{Liq-Gold}} = 2.5$ Å, we observed liquid atoms adsorbed in every fcc lattice position on any small (100) surface of the gold nanoparticle, this was not the case for $\sigma_{\mathrm{Liq-Gold}} = 3.65$ Å where the size of the adsorbent prevented this, and only allowed for much wider spaced absorption on the gold surface. Presumable this would destabilize non-hexagonal surfaces, causing only polymorphic Ih to be stable.

To summarize the results for nanoparticles grown in LJ liquids, we can say that we observed mostly Ih nanoparticles for low strengths adsorbents, and a mixture of Ih with some mDh, fcc based nanostructures for higher strength adsorbents, where solvent liquid densities roughly matched Gold's lattice constant. The overall trend tended to be in favor of non-Ih nanoparticle production when surface tensions are lowered. We can roughly compare these results with nanoparticles grown in vacuum and LJ noble gas vapors, were we found are Ih morphology to be the most abundant followed by the mDh and then fcc based morphologies [13]—although it should be pointed out that we have not taken growth statistic here. Surprisingly we observed no new nanoparticles compared to these previous results [13]. It is assumed that while LJ adsorbents can lower the overall interfacial surface tension they cannot significantly lower the tension of any particular surface relative to another.

3.2 Using "surface-bond-counts"

In the second set of simulations all adsorbent-gold interactions were still pair based but differed from the LJ form, containing fluctuations to bias absorption to certain surfaces. All adsorbent–adsorbent interactions remained of the LJ type.

An adsorbent ad-atom on an Au surface has the number of nearest neighbours as shown in table 1. It should be noted that the (100) and (110) surfaces have larger numbers of 1st and 3rd nearest neighbours with smaller numbers of 2nd nearest neighbors, Hence, for an adsorbent pair potential we added a number of units of the Gaussian function $-\exp\left[-7(r - r_{\mathrm{nei}})^2\right]$ where r_{nei} was the distance of the 1st and/or 3rd neighbours to bias the adsorption on certain surfaces. In this way we attempted to bias surface adsorption to the (100) and (110) to enhance their stability (figure 2).

All of the simulation were carried out using LJ solutions with $\sigma_{\mathrm{Liq-Gold}} = 2.6–2.7$ Å and $\varepsilon_{\mathrm{Liq-Liq}} = 0.038–0.04$ eV. We carried out simulation using a variety of scaling strengths of the above surface biasing potentials. Again, we can note that we did not obtain any new nanoparticle morphologies, even though we believe we successful managed to stabilize the (100) surface. The nanoparticles observed were mostly Ih for low strength surface biasing adsorbents, and mDh, nanoprisims and Truncated Octahedral (TO) particles with a high surface density, small random surface facets/defects for higher strength adsorbents. The m-Dh particles seemed to be more

Table 1. Number of nearest neighbours for each face.

Nearest neighbors	*(111) surface*	*(100) surface*	*(110) surface*
1st	3	5	4
2nd	3	2	1
3rd	9	10	12

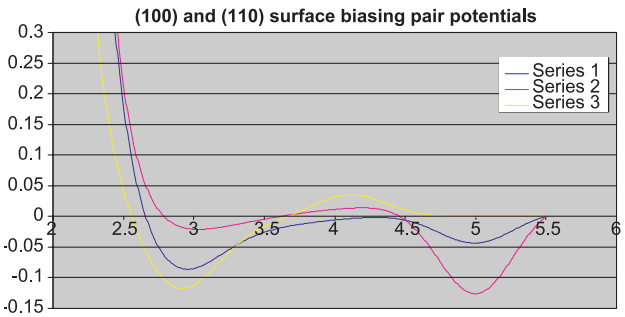

Figure 2. The (100) and (110) surface biasing pair potentials used showing energy versus seperation. Series 1, series 2 and series 3 are three potentials representative of those used.

abundant when grown in the (100) surface biasing potentials (although proper statistics gathering would need to be carried out to confirm this), with rounder aspects overall as compared with the "pancake" m-Dh particles which are grow in vacuum but, they contained strange randomly forming pyramid (or tetragonal) like facets all over with clearly visible (100) surfaces on their sides (figure 3). We can assume that in stabilizing the (100) face we have inadvertently stabilized the formation of such random (100) facets on the (111) face.

3.3 Effect of adding an adsorbent embedding function

Next we again attempted to bias absorption to certain surfaces based on the amount of gold electron density an ad-atom "feels" when adsorbed on certain surfaces. The adsorbent-gold pair potential contained a very sharp repulsive core to prevent embedding into the gold surface beyond a certain point. Adsorbents which adsorbed on the (110) surface received the most amount of electron density and could access the embedding well, while (111) surface adsorbents could not, see figure 4. We used many variants of this scheme which included the position of the shared repulsive core and the position of the adsorbent embedding well, and the inclusion of an attractive adsorbent pair potential.

These simulations were performed in an adsorbent vapour with some very interesting results. Firstly, some adsorbent schemes presumably stabilized the (110) and (100) surface to such an extent as to make the surface tension similar to the (111) (inferred from the observed population of visible surfaces). This resulted in nanoparticles with all manner of faces visible resembling a seemingly amorphous nanoparticle (figure 5(a)), which is not the case since internally (where the adsorbents cannot affect Au bonding) the nanoparticle was simply a m-Dh as

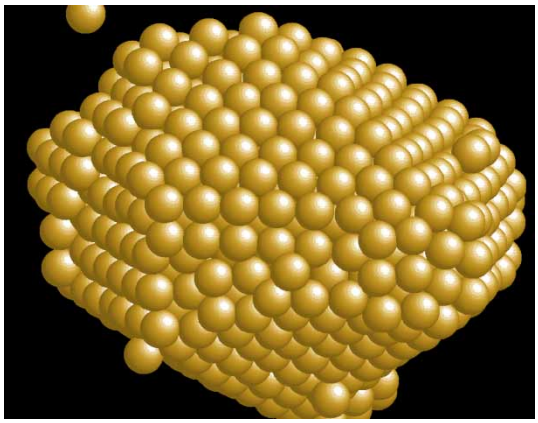

Figure 3. An early still somewhat "clean" Non-Pancake m-Dh. Note a two ad-atom high island has started to built up on the top left hand corner with (100) faces been clearly visible on all the islands sides, such islands continue to appear in random orientations for the (100) surface biased adsorbent growth.

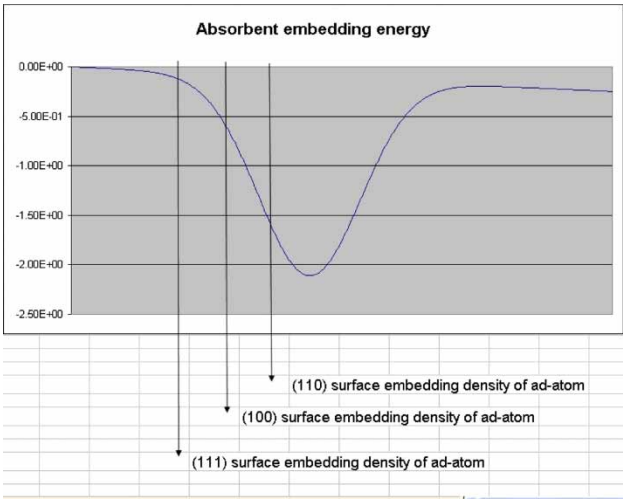

Figure 4. Embedding energy for adsorbent ad-atoms on the three gold surfaces (111), (100) and (110) showing the energy at the spacing for these surfaces.

can be seen from figure 5(b). Thus, the particle cores were ordered but the particle surfaces were disordered.

Other adsorbent schemes resulted in a simulation cell filled with only spherical nuclei of very similar sizes (figure 6) which happened due to an interesting repulsive effect that adsorbent atoms had on impinging gold atoms. This was that adsorbents which adsorb and embed in sufficient gold electron density (sufficiently supplied only by larger gold nuclei, as smaller nuclei have substantial surface curvature) will sit in their embedding well and will be repulsive to impinging gold atoms. This occurs since exposure to addition gold electron density would provide an excess of total embedding density making an adsorbent atom move out of its embedding energy well. This meant that once nuclei achieved a certain size and hence low curvature, adsorbent atoms would adsorb in significant numbers and drastically curtail growth. As can be seen from figure 6 small new nuclei have very little adsorbents attached leaving them fully open to growth while larger nuclei are saturated with adsorbents. This effect is very interesting and has the potential as a method of size control and will be followed up in future work.

Another adsorbent scheme included an attractive component to the adsorbent–adsorbent pair potential. This resulted in many different nanostructures, for example, if the well was centered at 3.8 Å then this presumably tended to order the adsorbent into a tight twisted (100) covering resulting in the growth of gold hexagonally twisted dendrite arms see figure 7. Again adsorbent atoms preferred to attach to low curvature gold surfaces and hence the tip of the dendrite arm, being a point of low curvature attracted little adsorbents and hence was exposed to further growth and elongation.

Yet other adsorbents preferred a hexagonal arrangement presumably forcing the gold structure into perfect fcc arrangements (figure 8(a),(b)). Some of the new nuclei

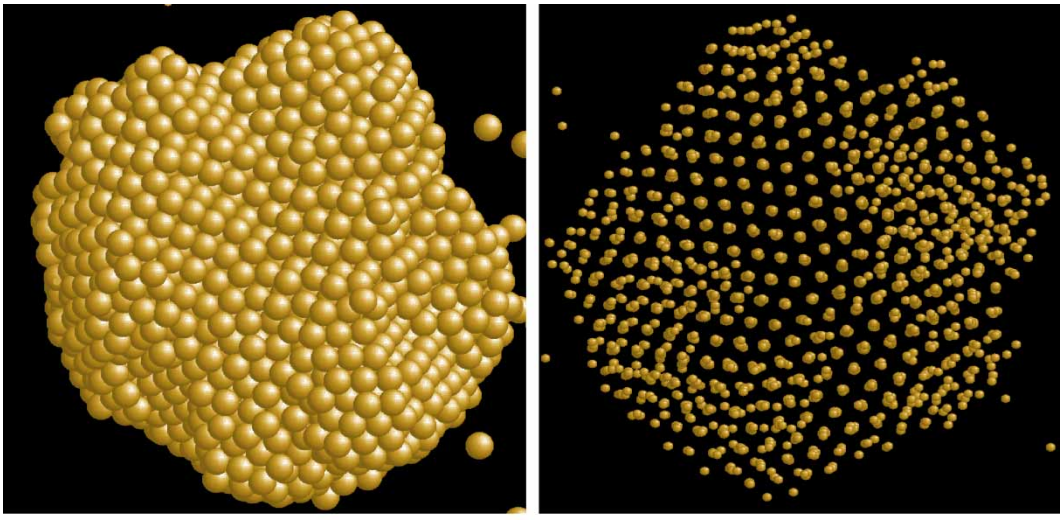

Figure 5. (a) and (b): a particle with a seemingly amorphous surface, shown in (a) but with an ordered core as shown in (b) looking down the five fold symmetric axis.

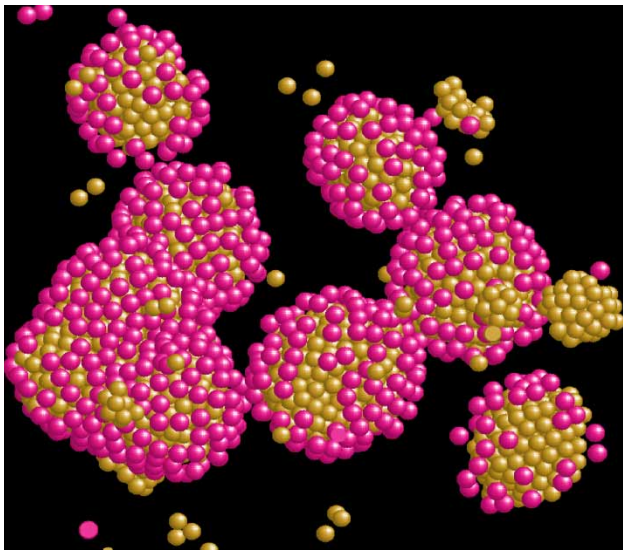

Figure 6. Many spherical nuclei of very similar size produced as discussed in Section 3.3.

were also forced into fcc like arrangements such as the fcc tetragonal structure shown in figure 8(b).

3.4 Supplying the surface Au with electron density

In this last series of simulations adsorbent atoms were allowed to contribute to the many body bonding of gold atoms by having an electron density function. The adsorbent-gold pair potential was chosen to be a weakly attractive LJ potential and all adsorbent–adsorbent interactions were very weakly LJ attractive. This is the only adsorbent which actually altered gold's surface bonding, as opposed to previous pair-wise absorbents which influence it indirectly though surface absorption. The purpose of choosing a very weak adsorbent–adsorbent interaction was so as to eliminate any adsorbent/vacuum surface tension. This type of adsorbent is expected to effectively reduce the surface free energy of the nanoparticle. Furthermore, we grew gold nanoparticles with a starting abundance of adsorbents, much more than is need to cover completely the initial nuclei.

The nanoparticles grown in these surface tension reducing vapour conditions were produced from eight identical growth simulations (where the only differing starting condition was the initial velocities) and we oobtained 5 m-Dh, 2 FCC and 1 Ih particle and, thus, we were able to change the previously found observance ratio completely and mostly grew rounder mDh particles with large areas of visible (100) surface. The characteristics of the nanoparticles was that all had very large concentration of surface defects,

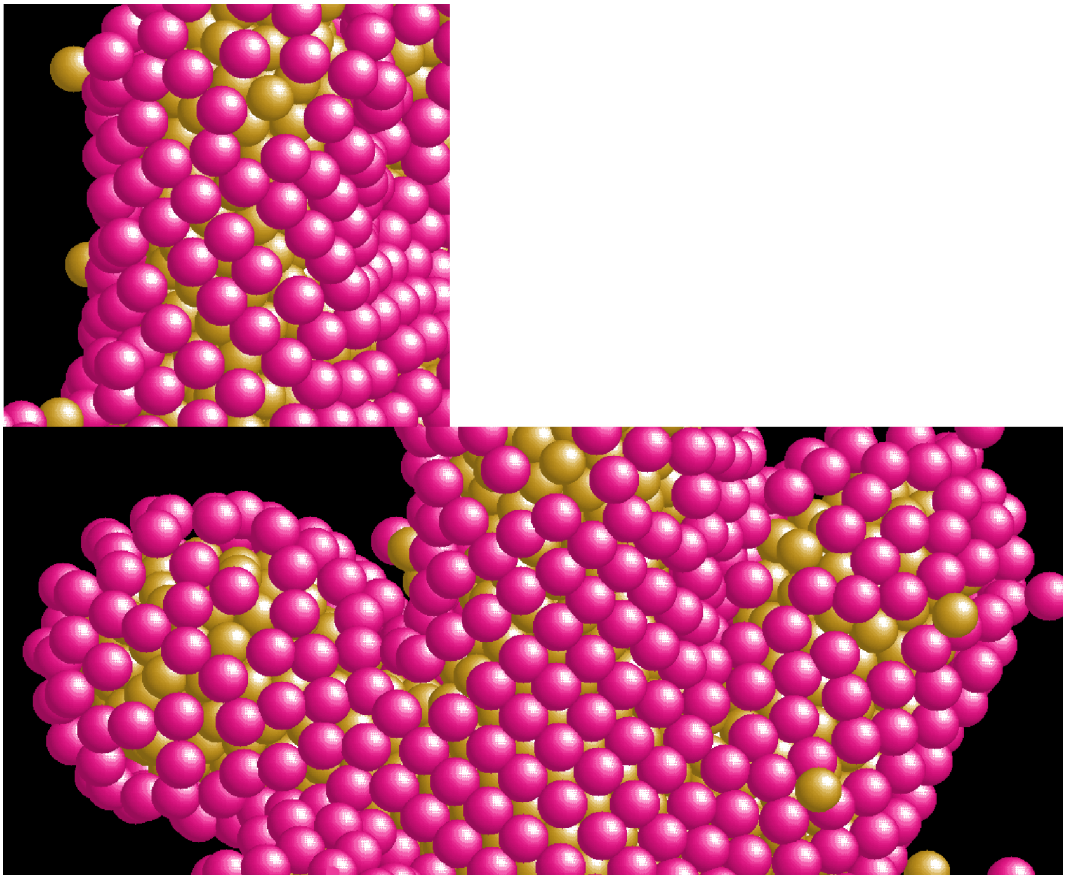

Figure 7. An example of a non-crystalline or twisted crystallize growth formation with dendrite-like arms. Note the twisted (100) adsorbent arrangement.

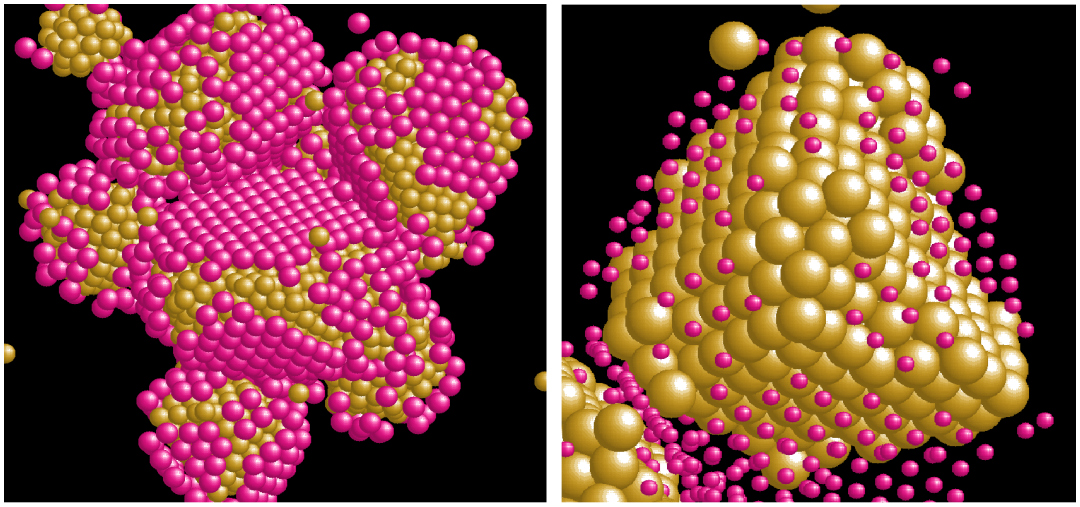

Figure 8. (a) and (b): new FCC tetragonal nanoparticles grown in stage 3 simulations, see Section 3.3.

presumably because the free energy associated with such defect was drastically reduced (figure 9).

4. Conclusion

MD growth simulations were preformed using various adsorbent types in the fluid and vapor phases to influence the growth mechanism of gold nanoparticles. We found a variety of interesting effects which can be used to influence the size and shape of nucleating nanoparticles.

However, we were unable to grow nano-rods and, in particular, structures with a predominance of (110) faces. Thus, in future work we will use a combination of two different types of adsorbents as well as adsorbents which have two different ends in an attempt to grow Au nanoparticles of other morphologies. Future work shall also focus on taking actual morphology statistics for each type of adsorbent and cataloging new nanoparticle morphologies.

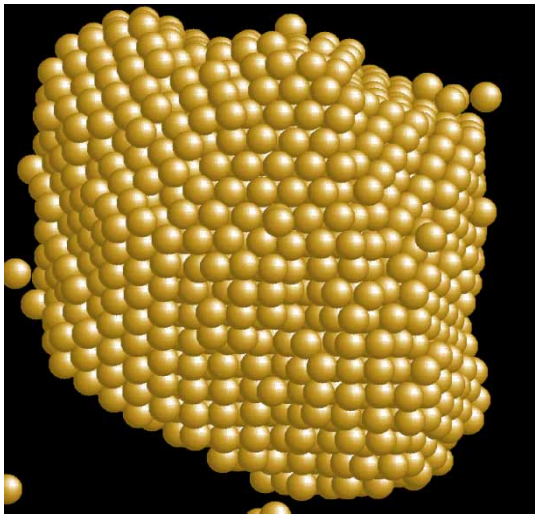

Figure 9. A round m-Dh particle with elongated (100) face produced in stage four, see Section 3.4.

References

[1] G. Opletal, T. Petersen, I. Snook, D. McCulloch, I. Yarovsky. Hybrid approach for generating realistic amorphous carbon structure using metropolis and reverse Monte Carlo. *J. Phys.: Condensed Matter*, **17**, 1 (2005).
[2] M.S. Dresselhaus, G. Dresselhaus, P. Eklund. *The Science of Fullerenes and Carbon Nanotubes*, Academic Press, London (1996).
[3] A.S. Barnard, S.P. Russo, I.K. Snook. Modeling of stability and phase transformations in 0 and 1 dimensional nanocarbon systems, Chapter 36. In *Handbook of Theoretical and Computational Nanotechnology*, M. Rieth, W. Schommers (Eds.), American Scientific Publishers, (2005).
[4] A.S. Barnard, S.P. Russo, I.K. Snook. Modeling of stability and phase transformations in quasi-zero dimensional nanocarbon systems. *J. Comp. Theo. Nanosci.*, **2**, 180 (2005).
[5] I.K. Snook, A.S. Barnard, S.P. Russo, R. Springall, J. Srbinovsky. Simulating nano-carbon materials. *Molec. Sim.*, **31**, 495 (2005).
[6] J.J. Wang, M.Y. Zhu, R.A. Outlaw, X. Zhao, D.M. Manos, D.M. Mammana, V.P. Mammana. Free-standing subnanometer graphite sheets. *Appl. Phys. Lett.*, **85**, 1265 (2004).
[7] G. Grochola, S.P. Russo, I.K. Snook. Application of the constrained fluid λ-integration path to the calculation of high temperature Au(110) surface free energies. *J. Chem. Phys.*, **122**, 064711 (2005).
[8] G. Grochola, S.P. Russo, I.K. Snook. On the computational calculation of surface free energies for the disordered semihexagonal reconstructed Au(100) surface. *J. Chem. Phys.*, **122**, 174510 (2005).
[9] K. Koga, K. Sugurawara. Population statistics of gold nanoparticles morphologies: direct determination by HREM observations. *Surf. Sci.*, **529**, 23 (2003).
[10] P.L. Gai, M.A. Harmer. Surface atomic defect structures and growth of gold nanorods. *Nano Lett.*, **7**, 771 (2002).
[11] Y. Sun, B. Mayers, Y. Xia. Metal nanostructures with hollow interiors. *Adv. Mater.*, **15**, 641 (2003).
[12] G. Grochola, S.R. Russo, I.K Snook. On fitting a gold embedded atom method potential using the force matching method. *J. Chem. Phys.*, **123**, 204719 (2005).
[13] G. Grochola, S.P. Russo, I.K. Snook. Observations on gold nanoparticle morphologies grown using molecular dynamics simulation, submitted to Phys. Rev. Lett.